


Study on Estimation Errors in ZUPT-Aided Pedestrian Inertial Navigation Due to IMU Noises

YUSHENG WANG , Student Member, IEEE
University of California, Irvine, USA

ANDREI CHERNYSHOFF 
L3 Technologies, Irvine, USA

ANDREI M. SHKEL, Fellow, IEEE
University of California, Irvine, USA

We present a study on the effects of the inertial measurement unit (IMU) noises on the navigation solution uncertainty during zero-velocity-update (ZUPT)-aided pedestrian inertial navigation. The analytically derived attitude, velocity, and position propagation errors reveal that among many IMU noise terms, the dominant factor affecting the accuracy of ZUPT-aided pedestrian navigation is rate random walk of gyroscopes. A numerical simulation has been conducted, showing the discrepancy of less than 10% between the numerical and analytical results, supporting fidelity of the analytical estimates. Experiments have also been conducted, and the results were on the same level of analytical and numerical predictions. This article offers a closed-form analytical prediction for the errors of ZUPT-aided pedestrian inertial navigation due to IMU noises.

Manuscript received November 19, 2018; revised May 15, 2019 and August 20, 2019; released for publication September 26, 2019. Date of publication October 18, 2019; date of current version June 9, 2020.

DOI. No. 10.1109/TAES.2019.2946506

Refereeing of this contribution was handled by S. Khanafseh.

This work was supported by the U.S. Department of Commerce, National Institute of Standards and Technology, under Award 70NANB17H192.

Authors' addresses: Y. Wang and A. M. Shkel are with the Department of Mechanical and Aerospace Engineering, University of California, Irvine, CA 92697 USA, E-mail: (yushengw@uci.edu; andrei.shkel@uci.edu.); A. Chernyshoff is with L3 Technologies, Irvine, CA 92603 USA, E-mail: (andrei.chernyshoff@gmail.com). (*Corresponding author: Yusheng Wang.*)

0018-9251 © 2019 IEEE

I. INTRODUCTION

The rapid development of the microelectromechanical-system-based inertial measurement units (IMUs) has made pedestrian inertial navigation possible for positioning in environments, where the global navigation satellite system is unavailable [1]. This approach is called pedestrian dead reckoning, since it does not depend on preinstalled infrastructure, such as GPS, long-term evolution, Bluetooth, radio frequency identification, and Wi-Fi signals [2]–[5]. The relation between IMU performance and accumulated navigation errors has also been widely studied and used as a guideline to improve the navigation accuracy by reducing IMU errors [6]. Unfortunately, low-cost IMUs has been suffering from a high noise level and low short-term and long-term stability, and these errors accumulate during the inertial navigation process. Without an error-suppressing algorithm, the position error accumulates approximately proportional to the time cubed and will exceed a meter of error within a few seconds of navigation for consumer-grade IMUs [7].

Many aiding techniques have been developed to be fused with inertial navigation to improve the navigation accuracy. Magnetometry is one of the most commonly used techniques, where the heading angle can be extracted from the measurement of the vector Earth magnetic field, if the roll and pitch angles are available from the measurement of the gravity [8]. Measuring orientation instead of the angular rate, as in most commercial gyroscopes, eliminates the angle drifts, which is a major source of navigation errors in dead reckoning. However, it requires a “magnetically clean place” to operate, which limits its applicability [9]. Another way of implementing estimations of absolute position is a computer vision. Images are captured and matched against the preacquired database for localization [10]. This approach potentially requires very large databases of the environment. The simultaneous location and mapping method has also been developed, which does not require a preacquired database. However, this method requires intensive calculation, and it mostly deals with static environment and suffers from odometry drifts [11]. Barometers are widely used to measure the altitude of the system during navigation [12]. This aiding technique is simple but is vulnerable to the disturbance of environmental pressure [13] and is only limited to measurements along the vertical direction. Ranging sensors have also been investigated to be implemented in pedestrian navigation, in the form of cooperative ranging between agents [14], foot-to-foot ranging [15], and directional ranging [16]. Ranging sensors measure the distance between the sensors, and it is, therefore, a relative measurement, resulting in a limited observability and thus a limited improvement of navigation accuracy [17].

Another widely used technique to suppress errors in pedestrian navigation is the zero-velocity-update (ZUPT)-aided navigation algorithm [18]–[20]. During the stance phase of pedestrian walking cycles, the foot periodically returns to a stationary (zero-velocity) state when it touches the ground. The ZUPT-aided navigation algorithm takes

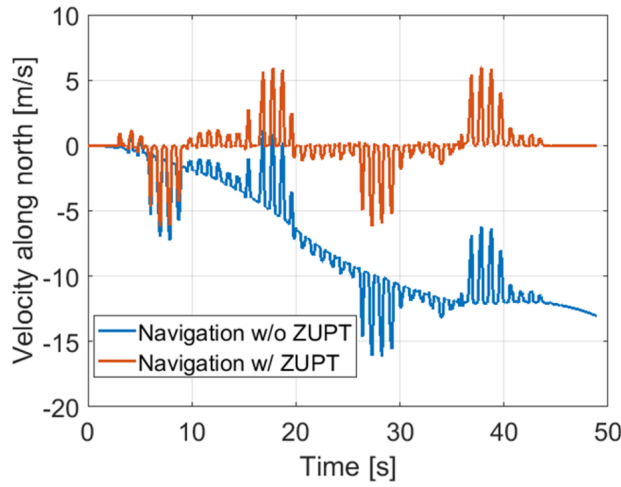


Fig. 1. Comparison between velocity estimations with and without the ZUPT-aided navigation algorithm. Changes in sign correspond to changes in the direction of motion.

advantage of this fact and uses the zero-velocity information during the stance phase as a pseudomeasurement fed into the extended Kalman filter (EKF) to compensate for IMU biases, thus reducing the navigation error growth in the system. It has been demonstrated that the ZUPT-aided navigation algorithm suppresses the cubic-in-time navigation error growth to a lower order of error growth and renders foot-mounted pedestrian navigation a great potential for practical use [21], [22]. Other assumptions during the stance phase, such as zero angular rate of the foot [23], and pure rotation of the foot around a pivot point near the toes [15], have been proposed, but they have not been widely accepted. Although the concept of ZUPT is simple and many studies have been conducted to demonstrate its effect on navigation errors, to the best of our knowledge, no analytical work has been conducted to quantify errors of ZUPT-aided navigation. Both systematic modeling errors and IMU noises were identified as the main error sources in ZUPT-aided inertial navigation [24]. In this article, we focus on the navigation errors related to the IMU noises, specifically to the white noise and stochastic bias of accelerometers and gyroscopes. The relation between white noises of accelerometers and gyroscopes of IMU and the root-mean-square error of ZUPT-aided inertial navigation has been *numerically* studied, and qualitative conclusions have been drawn in [25]. This article intends to fill the gap by *analytically* studying the navigation performance in the ZUPT-aided inertial navigation algorithm, relating the aforementioned noises to navigation accuracy, in terms of attitude, velocity, and position error.

II. IMPLEMENTATION OF THE ZUPT-AIDED ALGORITHM

The ZUPT-aided navigation algorithm takes advantage of the stance phase in a human gait cycle to compensate for the IMU drifts. The effects of the aiding on navigation are demonstrated in Fig. 1. Due to stochastic and deterministic

errors of the IMU, velocity of the foot would drift without usage of the ZUPT aiding, as presented by the blue line. However, the ZUPT-aided navigation algorithm helps to set the velocity of the foot close to zero during the stance phase and greatly reduces the effects of the IMU biases.

We implemented a standard strapdown inertial navigation system (INS) mechanization in the navigation frame. Drift correction was performed by implementing EKF operating on the error states $\delta\vec{x} = [\delta\vec{\theta}^T, \delta\vec{v}_n^T, \delta\vec{s}_n^T, \delta\vec{x}_g^T, \delta\vec{x}_a^T]^T$, where $\delta\vec{\theta}$ is the three-axis attitude error in the navigation frame, $\delta\vec{v}_n$ and $\delta\vec{s}_n$ are the vectors of velocity and position errors along the North, East, and Down directions of the navigation coordinate frame, $\delta\vec{x}_g$ is the gyroscope states (12-element vector) modeling gyroscope bias, scale factor error, rotational, and nonorthogonality misalignment, and $\delta\vec{x}_a$ is the accelerometer states (nine-element vector) modeling accelerometer bias, scale factor error, and nonorthogonality misalignment [26]. System state errors could be estimated by the EKF and compensated. A full dynamic error model could be approximated by

$$\delta\dot{\vec{x}} = \begin{bmatrix} -[\vec{\omega}_i^n \times] & F_{\delta v}^{\delta\theta} & 0 & -F_g & 0 \\ [\vec{f}^n \times] & C_1 & C_2 & 0 & F_a \\ 0 & I & 0 & 0 & 0 \\ 0 & 0 & 0 & 0 & 0 \\ 0 & 0 & 0 & 0 & 0 \end{bmatrix} \delta\vec{x} + \begin{bmatrix} C_{s_g}^n \cdot \epsilon_{ARW} \\ C_{s_a}^n \cdot \epsilon_{VRW} \\ 0 \\ \epsilon_{b_g} \\ \epsilon_{b_a} \end{bmatrix} \quad (1)$$

where $[\vec{\omega}_i^n \times]$ and $[\vec{f}^n \times]$ are the skew-symmetric cross-product operators of angular rate of the navigation frame relative to the inertial frame expressed in the navigation frame and of accelerometer output in the navigation frame, respectively. I is the identity matrix. $F_{\delta v}^{\delta\theta}$ is the term related to the transport rate, C_1 and C_2 are the terms related to the Coriolis effects due to the Earth rotation and the transport rate, $C_{s_g}^n$ and $C_{s_a}^n$ are the directional cosine matrices (DCMs) from the navigation frame to the coordinate frames of accelerometers and gyroscopes, respectively. F_g and F_a are matrices (3×12) and (3×9) modeling the linearized dynamics of the states $\delta\vec{x}_g$ and $\delta\vec{x}_a$, respectively, ϵ_{ARW} is the angle random walk (ARW) of the gyroscopes, and ϵ_{VRW} is the velocity random walk (VRW) of the accelerometers. ϵ_{b_g} and ϵ_{b_a} are noise terms in the first-order Markov process in the modeling of the states $\delta\vec{x}_g$ and $\delta\vec{x}_a$, respectively [27].

For a typical IMU, scale factor errors and misalignments vary slowly during a single pedestrian inertial navigation process and can be approximated by bias errors. We assume that the calibration process before the navigation is able to remove all deterministic biases. Therefore, in this article, only stochastic bias errors and white noises (ARW for gyroscopes and VRW for accelerometers) were considered, and the Earth rotation and the transport rate were also neglected. The simplification of the error model yielded a shorter system state $\delta\vec{x} = [\delta\vec{\theta}^T, \delta\vec{v}_n^T, \delta\vec{s}_n^T, \delta\vec{b}_g^T, \delta\vec{b}_a^T]^T$, where $\delta\vec{b}_g$ is the biases of three gyroscopes and $\delta\vec{b}_a$ is the biases of three accelerometers. Note that biases are not systematic errors.

With these corrections, the dynamic error model became

$$\delta \dot{\vec{x}} = \begin{bmatrix} 0 & 0 & 0 & -C_b^n & 0 \\ [\vec{f}^n \times] & 0 & 0 & 0 & C_b^n \\ 0 & I & 0 & 0 & 0 \\ 0 & 0 & 0 & 0 & 0 \\ 0 & 0 & 0 & 0 & 0 \end{bmatrix} \delta \vec{x} + \begin{bmatrix} C_b^n \cdot \epsilon_{ARW} \\ C_b^n \cdot \epsilon_{VRW} \\ 0 \\ \epsilon_{RRW} \\ \epsilon_{AcRW} \end{bmatrix} \triangleq A \delta \vec{x} + B \quad (2)$$

where C_b^n is the DCM from the navigation frame to the body frame, which is assumed to be aligned with the sensor frame, ϵ_{RRW} is the rate random walk (RRW) of the gyroscopes, and ϵ_{AcRW} is the accelerometer random walk (AcRW) of the accelerometers.

For each time step, besides calculating the system states (position, velocity, and attitude) in the standard strapdown navigation algorithm, we also propagated the *a priori* covariance using

$$P_{k+1|k} = F_k P_{k|k} F_k^T + Q_k \quad (3)$$

where $P_{k+1|k}$ is defined as the estimation error covariance matrix at the $(k+1)$ th time step based on measurements through the k th time step, and F and Q are defined as

$$F = \exp\{A \cdot \Delta t\} \approx I + A \cdot \Delta t$$

$$Q = \text{Var}\{B B^T\} \cdot \Delta t$$

where Δt is the time duration of each accumulation in (3), and B is the process noise defined in (2). In the discrete form, the system state update could be expressed as

$$\delta \vec{x}_{k+1|k} = F_k \cdot \delta \vec{x}_{k|k}$$

where $\delta \vec{x}_{k|k}$ is the estimation error from the previous (k)th time step, and $\delta \vec{x}_{k+1|k}$ is the *a priori* estimation error at the current step. This is called the prediction step in the EKF.

To activate the update part of the EKF, a zero-velocity detector was needed to detect the stance phase in each gait cycle. The standard stance hypothesis optimal detector was applied [28]. In this method, both accelerometer readouts and gyroscope readouts were taken into consideration to detect the stance phase. During the stance phase, the magnitude of the specific force should be equal to the local gravity, and the angular rate of the foot should be zero. However, the direction of the gravity was unknown to the detector, and thus, its maximum likelihood estimate was used. During a time epoch consisting of W number of measurements, the mean square error of the gyroscope readouts and the mean square error of the accelerometer readouts subtracted by a vector with the magnitude of the gravity and the direction of the averaged specific force were calculated, weighted by the uncertainty of the measurements, summed up, and compared with the threshold T (dimensionless). If the value was less than the threshold, the stance phase was detected. In the case of zero-velocity detection, the effect of false alarm was much worse than that of a miss-detection. Therefore, a proper combination of T and W was needed to minimize the probability of false detection at the cost of some miss-detection of the zero-velocity events. In this

article, W was set to be 5 and T was set to be 3×10^4 . The stance phase was detected if the variance was lower than the threshold value

$$\text{ZUPT} = H \left\{ \frac{1}{W} \sum_{k=1}^W \left(\frac{\|\mathbf{y}_k^a - g \cdot \mathbf{y}_k^{\bar{a}}\|^2}{\sigma_a^2} + \frac{\|\mathbf{y}_k^{\omega}\|^2}{\sigma_{\omega}^2} \right) - T \right\}$$

where ZUPT is the logical indicator of the detector, $H\{\cdot\}$ is the Heaviside step function, \mathbf{y}_k^a and \mathbf{y}_k^{ω} are accelerometer and gyroscope readouts at time step k , respectively, $\mathbf{y}_k^{\bar{a}}$ is the normalized and averaged accelerometer readout within the measurement window, σ_a and σ_{ω} are the white noise level of the accelerometers and gyroscopes of the IMU, respectively, and T is the threshold used in the detector.

When the stance phase was detected, the zero-velocity update was applied as pseudomeasurements, and velocity in the system state was considered as the measurement residual \vec{v}_k to update the state estimation

$$\vec{v}_k = \begin{bmatrix} 0 & I_{3 \times 3} & 0 \end{bmatrix} \cdot d\vec{x}_k + \vec{w}_k \triangleq H \cdot d\vec{x}_k + \vec{w}_k$$

where H is called the observation matrix, and \vec{w}_k is the measurement noise, which is mainly due to nonzero velocity of the IMU during the stance phase [29]. The covariance of \vec{w}_k is denoted by R_k . In most studies, \vec{w}_k was assumed to be white with constant and isotropic standard deviation r , which was generally set in the range from 0.001 to 0.1 m/s [18], [29]–[31]. The value r is also called velocity uncertainty. Therefore, the noise covariance matrix can be expressed as $R_k = r^2 I_{3 \times 3}$. In this article, we set the velocity uncertainty to be 0.02 m/s unless otherwise stated. This value matches the experimental data reported in [29].

After EKF receives the measurement information, it updates the system state with

$$\delta \vec{x}_{k+1|k+1} = \delta \vec{x}_{k+1|k} + K_{k+1} \cdot \vec{v}_{k+1} \quad (4)$$

where $\delta \vec{x}_{k+1|k+1}$ is the *a posteriori* estimation error, K_{k+1} is called the Kalman gain and calculated as

$$K_{k+1} = P_{k+1|k} H_{k+1}^T (H_{k+1} P_{k+1|k} H_{k+1}^T + R_{k+1})^{-1} \quad (5)$$

and the *a posteriori* covariance matrix has the form

$$P_{k+1|k+1} = (I - K_{k+1} H_{k+1}) P_{k+1|k}. \quad (6)$$

This is called the update step in the EKF, and it completes the iteration from time step k to $k+1$.

III. NAVIGATION ERROR ANALYSIS

The navigation errors in the ZUPT-aided navigation algorithm come mainly from two major sources: systematic modeling errors and IMU noises. We emphasize that in this article, we only analyze the navigation errors caused by IMU noises. In this section, we quantitatively analyze the navigation errors in terms of angle, velocity, and position.

A. Starting Point

A typical propagation of the error in attitude estimation in ZUPT-aided pedestrian inertial navigation and its covariance is presented in Fig. 2. A similar phenomenon

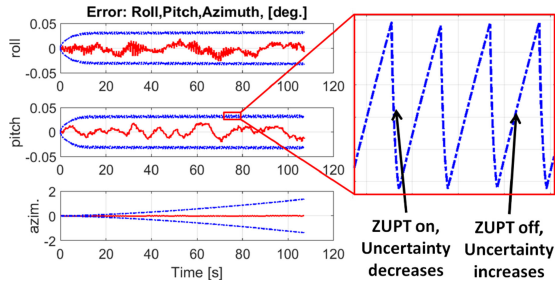


Fig. 2. Typical propagation of errors in attitude estimations in ZUPT-aided pedestrian inertial navigation. The red solid lines are the actual estimation errors, and the blue dashed lines are the 3σ uncertainty of estimation. Azimuth angle (heading) is the only important EKF state that is not observable from zero-velocity measurements.

can be observed for the velocity error propagation as well. A few conclusions can be drawn from propagation of errors in attitude estimation.

- 1) Although the propagated error is random due to the stochastic nature of noise (red solid lines in Fig. 2), the error covariances (bounds) follow a pattern (blue dashed lines in Fig. 2).
- 2) For roll and pitch angles, the covariance reaches a constant and the same level with some fluctuations, but covariance of azimuth angle propagates as $t^{1.5}$ due to RRW and lack of observability in azimuth angle [32].
- 3) The covariances are reduced if the update step is activated during the stance phase, and they are increased in the prediction step during the swing phase.

A starting point of the analysis was an observation that covariances of attitude and velocity reached a stable level with some fluctuation in the long run of the ZUPT-aided navigation algorithm [33], as shown by the blue dashed lines in Fig. 2. This observation indicated that in a whole gait cycle, the amount of the covariance increase in the prediction step was equal to the amount of the covariance decrease in the update step. Following this observation, we combined the parameters related to ZUPT and the IMU parameters to estimate the overall navigation solution uncertainty. This combination enabled us to fully analyze the system behavior and extract the covariance of the error in the system state estimation. For simplicity of derivation, we assumed in the analysis a straight line trajectory toward the North. We also assumed two-dimensional (2-D) motion of the foot: the foot only moves along the North and Down directions, and roll and azimuth angles are zero. In case of any other trajectory shapes, the analytical expression for the navigation error might be different, but the general conclusions would still hold.

B. Covariance Increase During Swing Phase

Covariance increases during the swing phase due to the noise in IMU readouts. The *a priori* covariance propagates according to (3). To differentiate the errors terms in position, velocity, and orientation, we expanded (3) into 3×3 subblocks, suppressed subscripts indicating the time steps for simplicity, and used new subscripts to indicate the

index of subblocks. In this way, subscript 1 corresponds to the angle error, subscript 2 corresponds to the velocity error, and subscript 3 corresponds to the position error. The *a priori* covariance propagation of angle in a single time step could be estimated by

$$P_{11}^{\text{priori}} \approx P_{11} + Q_{11} - (C_b^n P_{41} + P_{14} C_b^{nT}) \cdot \Delta t + C_b^n P_{44} C_b^{nT} \cdot \Delta t^2 \quad (7)$$

where Δt is the length of a time step. $C_b^n P_{41}$ and $P_{14} C_b^{nT}$ are symmetric with respect to each other and share the same on-diagonal terms. Note that in Sections III-B and III-C, terms in the form of P_{mn} and $P_{mn}(j, k)$ stand for the *a posteriori* covariance obtained from previous update step, or *a priori* covariance from previous prediction step if there is no update in the previous step. The last term on the right-hand side of (7) can be neglected, since the sampling rate is high (typically above 100 Hz). The high sampling frequency also helps to mitigate the error caused by applying the EKF to a nonlinear problem. Due to the assumption that the foot motion is 2-D, the DCM can be expressed by

$$C_b^n = \begin{bmatrix} \cos \theta & 0 & \sin \theta \\ 0 & 1 & 0 \\ -\sin \theta & 0 & \cos \theta \end{bmatrix}$$

where θ is the pitch angle of the foot. Since the orientation covariance propagations of the two horizontal directions (roll and pitch) were identical, we only needed to focus on one of them. In this article, we selected $P_{11}(1, 1)$, which corresponded to the roll angle, and its *a priori* covariance increase during the whole gait cycle was

$$P_{11}^{\text{priori}}(1, 1) \approx P_{11}(1, 1) + (ARW^2 - 2a_c P_{41}(1, 1)) \cdot t_{\text{stride}} \quad (8)$$

where t_{stride} is the time duration of a gait cycle, a_c is the averaged value of $\cos \theta$ during the whole gait cycle, and it is estimated to be around 0.84 for a normal human gait pattern [34]. $P_{41}(3, 1)$ was neglected because it is much smaller than $P_{41}(1, 1)$.

Covariance propagation of the velocity estimation error could be analyzed in a similar way based on (3):

$$P_{22}^{\text{priori}} \approx P_{22} + Q_{22} + \left\{ [\vec{f}^n \times] P_{12} + P_{21} [\vec{f}^n \times]^T + C_b^n P_{52} + P_{25} C_b^{nT} \right\} \Delta \quad (9)$$

P_{12} and P_{21} are symmetric with respect to each other. Integration of (9) over a whole gait cycle leads to the increase of the covariance of velocity estimation during a single gait cycle. $[\vec{f}^n \times]$ is composed of two parts: the constant acceleration \vec{g} and the fast-varying acceleration \vec{a}_m caused by motion. The latter can be neglected in the integration because P_{12} is a relatively slowly varying term compared to \vec{a}_m , and therefore, P_{12} could be considered constant in the integral of their multiplication in (9) and taken out of the integral. Therefore, the expression became an integral of the acceleration \vec{a}_m , which equals zero since the velocity returns to its original value in a complete gait

cycle. The terms $P_{52}(1, 1)$ and $P_{52}(1, 3)$ were much smaller than $P_{12}(1, 2)$ and thus could be neglected. Therefore, a total *a priori* covariance increase of the velocity error along the North could be expressed as

$$P_{22}^{\text{priori}}(1, 1) \approx P_{22}(1, 1) + (\text{VRW}^2 - 2g \cdot P_{12}(1, 2)) \cdot t_{\text{stride}} \quad (10)$$

where $P_{12}(1, 2)$ is the covariance between rotation along the North and the velocity along the East, and g is the gravitational acceleration. $P_{12}(1, 2)$ is an important parameter because it corresponds to coupling between the angular rate error and the velocity error. Schuler pendulum, for example, is one of the effects of this term [6]. To complete the analysis, we also need to calculate the covariance increase of $P_{12}(1, 2)$. The covariance propagation is described as

$$P_{12}^{\text{priori}}(1, 2) \approx P_{12}(1, 2) - g \cdot P_{11}(1, 1) \cdot t_{\text{stride}}. \quad (11)$$

The subblock in the covariance matrix that corresponded to the position estimation error is P_{33} , and its propagation in the prediction step could be expressed as

$$P_{33}^{\text{priori}} = P_{33} + (P_{23} + P_{32}) \cdot \Delta t + P_{22} \cdot \Delta t^2. \quad (12)$$

The position estimation uncertainties along the North and the East are represented by $P_{33}(1, 1)$ and $P_{33}(2, 2)$, respectively, and they only depend on the propagation of $P_{23}(1, 1)$ and $P_{23}(2, 2)$, which correspond to coupling between the velocity errors and position errors. Propagations of the coupling terms are expressed as

$$P_{23}^{\text{priori}}(1, 1) \approx P_{23}(1, 1) + [P_{22}(1, 1) + (g - a_D) \times P_{13}(2, 1)] \cdot \Delta t \quad (13)$$

$$P_{23}^{\text{priori}}(2, 2) \approx P_{23}(2, 2) + [P_{22}(2, 2) + (g - a_D)P_{13}(2, 1) - a_N P_{13}(3, 2)] \cdot \Delta t \quad (14)$$

where a_N is the acceleration along the North, and a_D is the acceleration toward the Down direction. Note that terms related to P_{53} were neglected and not shown in these equations. The reason why a_N and a_D cannot be neglected as in (10) will be explained later in this article. The only difference between the two directions is the last term in (14).

Similarly, propagations of covariance of other terms are

$$P_{12}^{\text{priori}}(3, 2) = P_{12}(3, 2) - P_{11}(3, 3) \cdot a_N \cdot \Delta t \quad (15)$$

$$P_{13}^{\text{priori}}(2, 1) = P_{13}(2, 1) + P_{12}(2, 1) \cdot \Delta t \quad (16)$$

$$P_{13}^{\text{priori}}(3, 2) = P_{13}(3, 2) + [P_{12}(3, 2) + \sin\theta P_{43}(1, 2) - \cos\theta P_{43}(3, 2)] \cdot \Delta t \quad (17)$$

$$P_{41}^{\text{priori}}(1, 1) = P_{41}(1, 1) - P_{44}(1, 1)\cos\theta \cdot \Delta t \quad (18)$$

$$P_{41}^{\text{priori}}(1, 3) = P_{41}(1, 3) + P_{44}(1, 1)\sin\theta \cdot \Delta t \quad (19)$$

$$P_{41}^{\text{priori}}(3, 3) = P_{41}(3, 3) - P_{44}(3, 3)\cos\theta \cdot \Delta t \quad (20)$$

$$P_{42}^{\text{priori}}(1, 2) = P_{42}(1, 2) + P_{41}(1, 1) \cdot (-g + a_D) \cdot \Delta t \quad (21)$$

$$P_{42}^{\text{priori}}(3, 2) = P_{42}(3, 2) - P_{41}(3, 3) \cdot a_N \cdot \Delta t \quad (22)$$

$$P_{43}^{\text{priori}}(1, 2) = P_{43}(1, 2) + P_{42}(1, 2) \cdot \Delta t \quad (23)$$

$$P_{43}^{\text{priori}}(3, 2) = P_{43}(3, 2) + P_{42}(3, 2) \cdot a_N \cdot \Delta t \quad (24)$$

$$P_{44}^{\text{priori}}(2, 2) = P_{44}(2, 2) + \text{RRW}^2 \cdot \Delta t. \quad (25)$$

C. Covariance Decrease During the Stance Phase

During the stance phase, the ZUPT-aided navigation algorithm compensates for the IMU errors/noise and, therefore, reduces the covariance of the state estimation. The amount of the total reduction can be calculated based on (5) and (6).

We first analyzed the covariance of the angle estimation. For each time step during the stance phase, the *a posteriori* covariance change could be expressed as

$$P_{11}^{\text{posteriori}}(1, 1) = P_{11}(1, 1) - \frac{P_{12}(1, 1)P_{21}(1, 1)}{P_{22}(1, 1) + r^2} - \frac{P_{12}(1, 2)P_{21}(2, 1)}{P_{22}(2, 2) + r^2} - \frac{P_{12}(1, 3)P_{21}(3, 1)}{P_{22}(3, 3) + r^2} \approx P_{11}(1, 1) - \frac{P_{12}(1, 2)^2}{r^2}. \quad (26)$$

In the strapdown inertial navigation mechanization, the rotation along the North is strongly coupled with the acceleration along the East due to the gravity. Therefore, $P_{12}(1, 1)$ and $P_{12}(1, 3)$ are much smaller than $P_{12}(1, 2)$ and could be neglected. The velocity measurement uncertainty is generally much greater than velocity error induced by IMU noises in the ZUPT-aided navigation process [24], [35]. As a result, P_{22} in the denominator is smaller than r^2 and could be neglected.

Similarly, *a posteriori* covariance of other terms that are needed in the derivation could be calculated as

$$P_{12}^{\text{posteriori}}(1, 2) = P_{12}(1, 2) - P_{12}(1, 2) \cdot P_{22}(2, 2)/r^2 \quad (27)$$

$$P_{22}^{\text{posteriori}}(2, 2) = P_{22}(2, 2) - P_{22}(2, 2)^2/r^2 \quad (28)$$

$$P_{13}^{\text{posteriori}}(3, 2) = P_{13}(3, 2) - P_{23}(2, 2) \cdot P_{12}(3, 2)/r^2 \quad (29)$$

$$P_{13}^{\text{posteriori}}(2, 1) = P_{13}(2, 1) - P_{23}(1, 1) \cdot P_{12}(2, 1)/r^2 \quad (30)$$

$$P_{33}^{\text{posteriori}}(1, 1) = P_{33}(1, 1) - P_{23}(1, 1)^2/r^2 \quad (31)$$

$$P_{22}^{\text{posteriori}}(1, 1) = P_{22}(1, 1) - P_{22}(1, 1)^2/r^2 \quad (32)$$

$$P_{33}^{\text{posteriori}}(2, 2) = P_{33}(2, 2) - P_{23}(2, 2)^2/r^2 \quad (33)$$

$$P_{44}^{\text{posteriori}}(2, 2) = P_{44}(2, 2) - P_{42}(2, 1)^2/r^2 \quad (34)$$

$$P_{42}^{\text{posteriori}}(1, 2) = P_{42}(1, 2) - P_{42}(1, 2)P_{22}(2, 2)/r^2 \quad (35)$$

$$P_{41}^{\text{posteriori}}(1, 1) = P_{41}(1, 1) - P_{42}(1, 2)P_{21}(2, 1)/r^2. \quad (36)$$

D. Covariance Level Estimation

Since the ZUPT-aided navigation algorithm has limited observability of azimuth angle, as shown in Fig. 2, the propagation of error in the azimuth angle and in the z -axis gyroscope bias is the same as in strapdown inertial navigation

$$P_{44}(3, 3) = \text{RRW}^2 \cdot t, \quad (37)$$

$$P_{11}(3, 3) = \text{ARW}^2 \cdot t + \frac{\text{RRW}^2}{3} \cdot t^3 \quad (38)$$

where t is the total navigation time. In Section III-D, terms in the form of P_{mn} and $P_{mn}(j, k)$ stand for the predicted continuous covariance bounds. Besides, in this section, we only focus on the level of covariance in the long term

and neglect the variance change within a single gait cycle. Therefore, we do not distinguish *a priori* and *a posteriori* covariances anymore.

A combination of (25) and (34) gives

$$\text{RRW}^2 \cdot t_{\text{stride}} = \frac{P_{42}(2, 1)^2}{r^2} \cdot N_{\text{stance}}. \quad (39)$$

Since $N_{\text{stance}} = f_s \cdot t_{\text{stance}}$, where f_s is the sampling frequency of the IMU, P_{42} can be expressed as

$$P_{42}(1, 2) = -\text{RRW} \left[\frac{r^2 \cdot t_{\text{stride}}}{f_s \cdot t_{\text{stance}}} \right]^{\frac{1}{2}}. \quad (40)$$

The minus sign in the equation was due to the fact that a positive gyroscope bias along the East would cause a negative velocity estimation error along the North.

Similarly, a combination of (21) and (35) gives

$$-P_{44}(1, 1) \cdot g \cdot t_{\text{stride}} = \frac{P_{42}(1, 2)P_{22}(2, 2)}{r^2} f_s \cdot t_{\text{stance}}. \quad (41)$$

A combination of (8) and (26) gives

$$[\text{ARW}^2 - 2a_c P_{41}(1, 1)] \cdot t_{\text{stride}} = \frac{P_{12}(1, 2)^2}{r^2} f_s \cdot t_{\text{stance}}. \quad (42)$$

A combination of (10) and (32) gives

$$[\text{VRW}^2 - 2g \cdot P_{12}(1, 2)] \cdot t_{\text{stride}} = \frac{P_{22}(1, 1)^2}{r^2} f_s \cdot t_{\text{stance}}. \quad (43)$$

From (40)–(43), we are able to calculate $P_{22}(1, 1)$, which is the root of a quartic equation

$$ax^4 + bx^2 + cx + d = 0 \quad (44)$$

with coefficients expressed as

$$a = \left[\frac{f_s \cdot t_{\text{stance}}}{2gr^2 \cdot t_{\text{stride}}} \right]^2, \quad b = -\frac{f_s \cdot t_{\text{stance}} \text{VRW}^2}{2g^2 r^2 \cdot t_{\text{stride}}}$$

$$c = -2a_c \frac{\text{RRW}}{g} \sqrt{\frac{r^2 t_{\text{stride}}}{f_s t_{\text{stance}}}}, \quad d = \frac{\text{VRW}^4}{4g^2} - \frac{\text{ARW}^2 r^2 t_{\text{stride}}}{f_s t_{\text{stance}}}.$$

An analytical solution to (44) exists, but it is too complicated and not instructive to write it here. Therefore, in this article, instead of searching for the analytical expression, we calculated the solution numerically. Note that $P_{22}(1, 1)$ is the term in the covariance matrix that corresponded to uncertainty of the velocity estimation along the East. The velocity uncertainty is simply $\sigma_v = \sqrt{P_{22}(2, 2)}$. From the above equations, $P_{12}(1, 2)$ and $P_{41}(1, 1)$ could be calculated as

$$P_{12}(1, 2) = -\left[\text{ARW}^2 \frac{r^2 t_{\text{stride}}}{f_s t_{\text{stance}}} + 2a_c \frac{\text{RRW} \cdot \sigma_v^2}{g} \sqrt{\frac{r^2 t_{\text{stride}}}{f_s t_{\text{stance}}}} \right]^{\frac{1}{2}} \quad (45)$$

$$P_{41}(1, 1) = -\frac{\text{RRW} \cdot \sigma_v^2}{g} \sqrt{\frac{f_s t_{\text{stance}}}{r^2 t_{\text{stride}}}}. \quad (46)$$

A combination of (18) and (36) gives

$$P_{44}(1, 1)a_c \cdot t_{\text{stride}} = \frac{P_{42}(1, 2)P_{21}(2, 1)}{r^2} f_s \cdot t_{\text{stance}} \quad (47)$$

i.e.

$$P_{44}(1, 1) = \frac{P_{42}(1, 2)P_{21}(2, 1)}{a_c} \frac{f_s \cdot t_{\text{stance}}}{r^2 \cdot t_{\text{stride}}} = \left[\left(\frac{\text{RRW} \cdot \text{ARW}}{a_c} \right)^2 + \frac{2\sigma_v^2 \text{RRW}^3}{a_c \cdot g} \sqrt{\frac{f_s t_{\text{stance}}}{r^2 t_{\text{stride}}}} \right]^{\frac{1}{2}}. \quad (48)$$

The uncertainty of gyroscope bias along the North is $\sigma_{gN} = \sqrt{P_{44}(1, 1)}$.

Attitude estimation covariance is obtained by combining (11) and (27) as

$$-P_{11}(1, 1) \cdot g \cdot t_{\text{stride}} = \frac{P_{12}(1, 2)P_{22}(2, 2)}{r^2} f_s \cdot t_{\text{stance}} \quad (49)$$

i.e.

$$P_{11}(1, 1) = -\frac{P_{12}(1, 2)P_{22}(2, 2)}{g} \frac{f_s \cdot t_{\text{stance}}}{r^2 \cdot t_{\text{stride}}}. \quad (50)$$

The uncertainty of the attitude estimation along the North is $\sigma_\theta = \sqrt{P_{11}(1, 1)}$.

To estimate the position uncertainty, we analyzed the propagation of $P_{12}(3, 2)$ first. Equation (15) shows that the propagation of $P_{12}(3, 2)$ is related to the acceleration along the North a_N and the azimuth angle uncertainty $P_{11}(3, 3)$. In a single gait cycle, $P_{11}(3, 3)$ can be considered as constant, since the duration of one gait cycle is relatively short (around 1 s). Thus, $P_{12}(3, 2)$ is an integral of a_N , i.e., the real velocity of IMU along the North $v_N(t)$. Therefore, $P_{12}(3, 2)$ returns to a near-zero value when the update step begins, and as a result, the update step has a little effect on $P_{12}(3, 2)$, since its value is already close to zero. $P_{12}(3, 2)$ can be expressed as

$$P_{12}(3, 2) \approx -P_{11}(3, 3) \cdot v_N(t) = -\left(\text{ARW}^2 t + \frac{\text{RRW}^2}{3} t^3 \right) \cdot v_N(t). \quad (51)$$

Similarly, several other terms that were necessary in the derivation can be calculated as

$$P_{41}(3, 3) = -\int_0^t P_{44}(3, 3) \cdot \cos\theta \cdot d\tau = -\frac{\text{RRW}^2}{2} \cdot a_c \cdot t^2$$

$$P_{41}(1, 3) = \int_0^t P_{44}(1, 1) \cdot \sin\theta \cdot d\tau = \sigma_{gN}^2 \cdot a_s \cdot t,$$

$$P_{42}(1, 2) = -\int_0^t P_{41}(1, 3) \cdot a_N \cdot d\tau = -\sigma_{gN}^2 \cdot a_s \cdot t \cdot v_N(t),$$

$$P_{42}(3, 2) = -\int_0^t P_{41}(3, 3) \cdot a_N \cdot d\tau = \frac{\text{RRW}^2}{2} \cdot a_c \cdot t^2 \cdot v_N(t)$$

$$P_{43}(1, 2) = \int_0^t P_{42}(1, 2) \cdot d\tau = -\int_0^t \sigma_{gN}^2 \cdot a_s \cdot t \cdot v_N(t) \cdot d\tau$$

$$\approx -\sum_i \sigma_{gN}^2 \cdot a_s \cdot t_i \int_{\text{cycle } i} v_N(t) \cdot d\tau$$

$$= -\sum_i \sigma_{gN}^2 \cdot a_s \cdot t_i s_N = -\frac{1}{2} \sigma_{gN}^2 \cdot a_s \cdot t^2 s_N$$

$$\begin{aligned}
P_{43}(3, 2) &= \int_0^t P_{42}(3, 2) \cdot d\tau = \frac{RRW^2}{6} \cdot a_c \cdot s_N \cdot t^3 \\
P_{13}(3, 2) &= \int_0^t [P_{12}(3, 2) + P_{43}(1, 2)\sin\theta \\
&\quad - P_{43}(3, 2)\cos\theta] d\tau \\
&= -\left(\frac{ARW^2}{2}t^2 + \frac{RRW^2}{12}t^4\right) \cdot s_N \\
&= -\frac{1}{6}\sigma_{g_N}^2 \cdot a_s^2 \cdot s_N \cdot t^3 - \frac{RRW^2}{24} \cdot a_c^2 \cdot s_N \cdot t^4
\end{aligned}$$

where a_s is the average value of $\sin\theta$ over the whole gait cycle, and s_N is the stride length of the human gait. In the equation for $P_{43}(1, 2)$, the integral over the whole navigation process was calculated as the summation of the integral over each gait cycle i . Besides, in the integral of each gait cycle, t was approximated as a constant t_i and moved out of the integral, because the relative changing rate of v_N was much larger than that of t in a single gait cycle.

Then, we estimate the level of P_{23} , since it is related to the propagation of P_{33} , both in the prediction step [indicated by (12)] and in the update step [indicated by (31) and (33)].

From our extensive observation of many cases, the value of $P_{13}(2, 1)$ remained at a constant level during the navigation. Therefore, a combination of (16) and (30) yields

$$P_{12}(2, 1)t_{\text{stride}} = N_{\text{stance}}P_{23}(1, 1) \cdot P_{12}(2, 1)/r^2 \quad (52)$$

or equivalently represents

$$P_{23}(1, 1) = \frac{r^2 \cdot t_{\text{stride}}}{N_{\text{stance}}} = \frac{r^2 \cdot t_{\text{stride}}}{f_s \cdot t_{\text{stance}}}. \quad (53)$$

Comparing (13) and (14) yields

$$\begin{aligned}
P_{23}(2, 2) &= P_{23}(1, 1) - \int_0^t a_N P_{13}(3, 2) \cdot d\tau \\
&\approx \frac{r^2 \cdot t_{\text{stride}}}{f_s \cdot t_{\text{stance}}} - P_{13}(3, 2) \cdot v_N(t). \quad (54)
\end{aligned}$$

Now, we explain the reason why the acceleration caused by foot motion cannot be neglected in (13) and (14). The position uncertainty $P_{33}(2, 2)$ was derived by integrating $P_{23}(2, 2)$ twice, and the acceleration term a_N would be transformed to the displacement term s_N . Therefore, even though the velocity v_N returned to zero after a full gait cycle, its integral, displacement s_N , cannot be neglected. The acceleration term in (10), however, was only integrated once to obtain the final result for velocity uncertainty. As a result, neglecting the acceleration term would not introduce large errors but would only lose information about some fluctuations within a single gait cycle.

Combining (12) and (31), we could obtain the full increment of $P_{33}(1, 1)$, which corresponded to the square of position uncertainty along the trajectory, during a complete gait cycle

$$\begin{aligned}
\Delta P_{33}(1, 1) &= 2P_{23}(1, 1) \cdot t_{\text{stride}} - P_{23}(1, 1)^2/r^2 \cdot N_{\text{stance}} \\
&\approx \left(2 - \frac{t_{\text{stride}}}{4}\right) \frac{r^2 \cdot t_{\text{stride}}}{f_s \cdot t_{\text{stance}}} \cdot t_{\text{stride}}. \quad (55)
\end{aligned}$$

Therefore, the propagation of $P_{33}(1, 1)$ can be expressed as

$$P_{33}(1, 1) = \left(2 - \frac{t_{\text{stride}}}{4}\right) \frac{r^2 \cdot t_{\text{stride}}}{f_s \cdot t_{\text{stance}}} \cdot t. \quad (56)$$

The propagation of $P_{33}(2, 2)$ can be derived similarly as

$$\begin{aligned}
P_{33}(2, 2) &= \left(2 - \frac{t_{\text{stride}}}{4}\right) \frac{t_{\text{stride}}r^2}{t_{\text{stance}}f_s} \cdot t + \frac{1}{3}ARW^2s_N^2 \cdot t^3 \\
&= +\frac{a_s^2}{12}\sigma_{g_N}^2s_N^2 \cdot t^4 + \left(\frac{1}{30} + \frac{a_c^2}{60}\right)RRW^2s_N^2 \cdot t^5. \quad (57)
\end{aligned}$$

Set $\sigma_{||} = \sqrt{P_{33}(1, 1)}$ and $\sigma_{\perp} = \sqrt{P_{33}(2, 2)}$. $\sigma_{||}$ and σ_{\perp} are the position estimation uncertainties parallel and perpendicular to the trajectory, and they correspond to 1.2 times of the semimajor and semiminor axes of circular error probable, respectively.

Equations (38), (44), (50), (56), and (57) fully describe the uncertainty of navigation results due to IMU noises with respect to angle, velocity, and position.

E. Comments

- 1) ARW, VRW, and RRW all affect the final navigation uncertainties, for example in (44); higher noise level results in larger errors.
- 2) The velocity measurement uncertainty r plays an important role in the final results; lower r indicates a higher reliability and weight of the zero-update information in EKF, resulting in a better navigation accuracy. However, this value is determined by human gait pattern and the type of floor [29]. Therefore, it should be adjusted according to the experiment and cannot be set arbitrarily.
- 3) The position uncertainty along the trajectory is dominated by the velocity measurement uncertainty r in the EKF and is proportional to square root of the navigation time.
- 4) The position uncertainty perpendicular to the trajectory depends on many parameters [see (57)]. However, it is dominated by RRW and is proportional to the navigation time of the power of 2.5, in the case of long-term navigation.
- 5) Human gait pattern affects the navigation errors. It is reflected in the ratio between duration of the stance phase and the whole gait cycle and the average of sine and cosine value of the pitch angle, for example in (42). A higher percentage of the stance phase during the gait cycle gives the EKF more data to compensate for the IMU noises and reduces the overall navigation errors.
- 6) The AcRW is not included in the model. This is due to our assumption that the propagated velocity covariance during the swing phase is much smaller than the velocity measurement uncertainty r . This conclusion is in sync with the argument in [24].
- 7) The results are only approximations of the navigation errors due to assumptions and approximations made

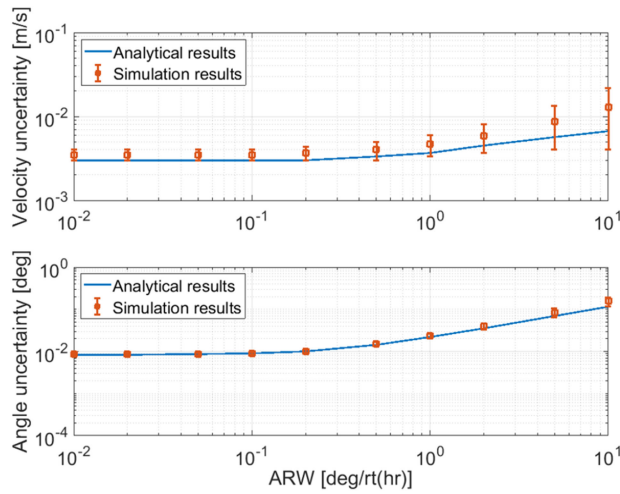


Fig. 3. Effects of ARW of the gyroscopes on the velocity and angle estimation errors in the ZUPT-aided navigation algorithm.

during the derivation, e.g., 2-D foot motion, moderate IMU performance, high IMU sampling rate, straight trajectory, etc. Validity of the approximations will be demonstrated in the following section.

IV. VERIFICATION OF ANALYSIS

A. Numerical Verification

Simulations were conducted to verify the derived analytical expressions. First, a trajectory of foot toward the North and the corresponding IMU readouts were generated based on a human gait analysis [35]. Then, the numerical results were compared to analytical expressions. The generated trajectory was a straight line toward the North containing 100 steps. The total time duration of the trajectory was 53.6 s, and the total length of the trajectory was 77 m.

1) *Effects of ARW*: We first studied the influence of ARW of gyroscopes on the navigation errors. We swept the ARW value from 0.01 to $10^\circ/\sqrt{\text{h}}$ (from near navigation-grade to consumer-grade), while keeping other parameters constant. VRW of accelerometers was set to be $0.14 \text{ mg}/\sqrt{\text{Hz}}$ (near tactical-grade), RRW of gyroscopes was set to be $0.048^\circ/\text{s}/\sqrt{\text{h}}$, and the sampling frequency was selected to be 800 Hz. The simulation results are presented in Fig. 3. The upper plot shows a relation between ARW and the velocity estimation uncertainty, and the lower plot shows a relation between ARW and the angle estimation uncertainty. Notice that the angle estimation uncertainty is only for roll and pitch angle, since the yaw angle is unobservable in the EKF and propagates according to (38). In both plots, the blue lines are analytical results, and the red error bars are simulation results. The simulation results are a range instead of a value because covariances of the estimation errors fluctuated during the navigation (see Fig. 2). The upper and lower bounds of the error bars showed the amplitude of fluctuation, and the square showed an average value of the fluctuation.

A close match between the analytical and simulation results verified the validity of the analysis. Fig. 3 showed

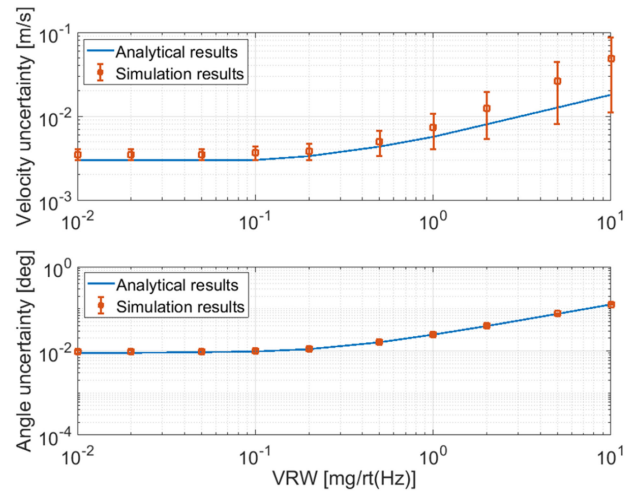


Fig. 4. Effects of VRW of the accelerometers on the velocity and angle estimation errors in the ZUPT-aided navigation algorithm.

that both the velocity estimation uncertainty and the angle estimation uncertainty were not affected by ARW when its value was smaller than $0.1^\circ/\sqrt{\text{h}}$. One possible reason was that in this case, the navigation uncertainty was dominated by other errors, such as VRW and RRW; therefore, it was independent of the ARW value. The lower bound of the fluctuation of velocity uncertainty was almost not affected by ARW either. This was because the lower bound of the velocity uncertainty was limited by the velocity measurement uncertainty set in the EKF, which was fixed in this model. It was also noticed that fluctuation of the angle uncertainty was much smaller than the velocity uncertainty. The reason was that the velocity was directly observable in the ZUPT-aided navigation algorithm, and therefore, the EKF could directly estimate the velocity value and reduce the velocity uncertainty. The angle estimation, however, was achieved through coupling the velocity and angle, and as a result, the observability was reduced.

2) *Effects of VRW*: Similarly, we swept the VRW value of accelerometers from 0.01 to $10 \text{ mg}/\sqrt{\text{Hz}}$, while keeping ARW of the gyroscope to be $0.21^\circ/\sqrt{\text{h}}$ (tactical grade) and RRW to be $0.048^\circ/\text{s}/\sqrt{\text{h}}$. The results are shown in Fig. 4. As expected, the curves became flat when VRW was small, since the navigation error was dominated by gyroscope errors in this range.

3) *Effects of RRW*: As indicated in (57), RRW is the major error source that affects the navigation accuracy. We swept the RRW value of gyroscopes from 0.6 to $600 \text{ mdeg}/\text{s}/\sqrt{\text{h}}$, while keeping ARW of the gyroscope to be $0.21^\circ/\sqrt{\text{h}}$ and VRW to be $0.14 \text{ mg}/\sqrt{\text{Hz}}$. The influence of RRW on the velocity and angle estimation errors is shown in Fig. 5.

Fig. 6 shows the relation between the position uncertainty and RRW. A difference within 10% was demonstrated between the analytical results and the numerical results. Note that the position uncertainty perpendicular to the trajectory is not affected by RRW, but dominated by velocity uncertainty during the stance phase. As a result, a lower

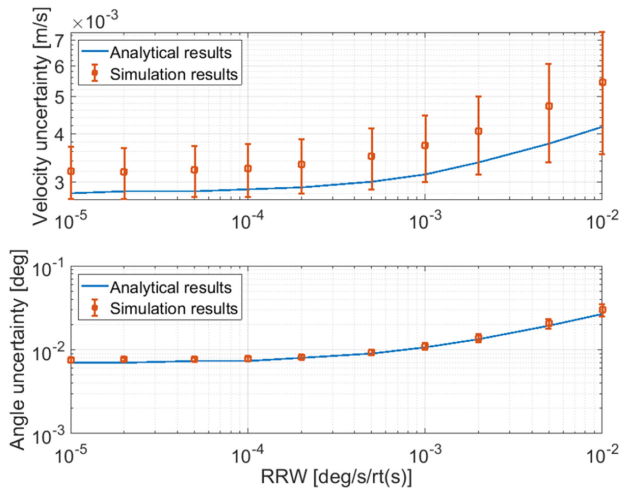


Fig. 5. Effects of RRW of the gyroscopes on the velocity and angle estimation errors in the ZUPT-aided navigation algorithm.

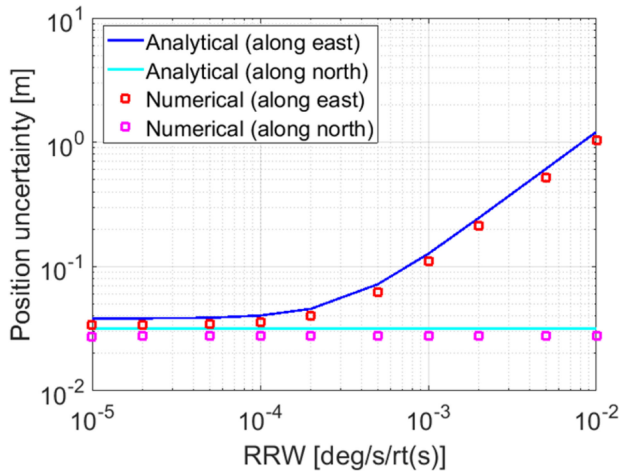


Fig. 6. Relation between RRW of gyroscopes and the position estimation uncertainties.

velocity measurement uncertainty would be desirable for a better navigation accuracy. The following considerations could help to reduce the velocity measurement uncertainty and improve the overall navigation accuracy: 1) a stiffer shoe with less deformation during walking; 2) a better position to attach the IMU, so that the IMU could be more stationary during the stance phase; and 3) shock absorber on the shoes to prevent strong shocks between the shoe and the ground.

B. Experimental Verification

A VectorNav VN-200 INS (near tactical-grade) was mounted on the right shoe by a 3-D printed fixture (see Fig. 8), and IMU readouts were collected during walking. The uncompensated IMU data instead of the compensated ones were used to avoid any possible effects of the filtering algorithm in the INS on the overall navigation accuracy. Allan deviations of the accelerometer and gyroscope readouts were collected to confirm the performance of the IMU [36], and the result is shown in Fig. 7. ARW, VRW,

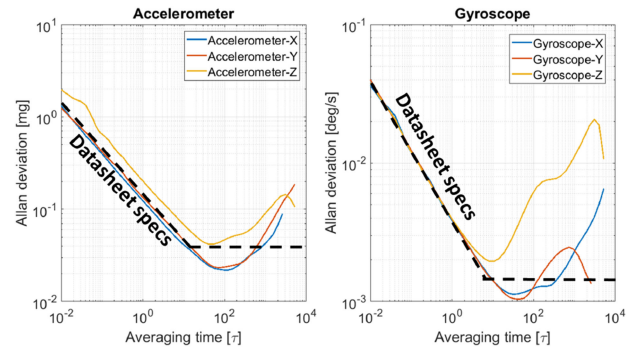


Fig. 7. Allan deviation plot of the IMU used in this study. The result is compared to the datasheet specs [37].

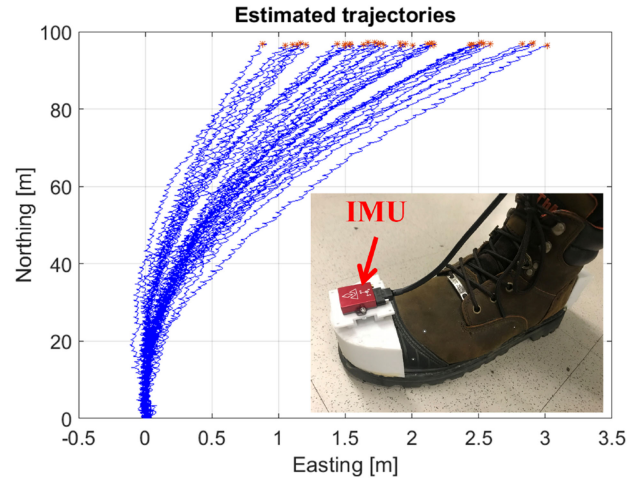


Fig. 8. Navigation error results of 40 trajectories. The averaged time duration was about 110 s, including the initial calibration. Note that scales for the two axes are different to highlight the effect of error accumulation.

and RRW of the IMU were $0.21^\circ/\sqrt{h}$, $0.14 \text{ mg}/\sqrt{\text{Hz}}$, and $0.048^\circ/\text{s}/\sqrt{\text{hr}}$, respectively. The sampling frequency was set to be 800 Hz (maximum sampling rate of the IMU) to capture the high-frequency component of the motion. The length of the straight line trajectory was around 100 m, and the total navigation time was around 110 s. During the first 10 s of each run, the foot was stationary for the initial calibration of the IMU. A magnetometer was used to determine the initial orientation of the foot. IMU data for 40 trajectories were collected to obtain a relatively accurate position uncertainty during the navigation.

The navigation error results of 40 trajectories are shown in Fig. 8. In all cases, the nominal trajectory is a straight line trajectory toward the North. All estimated trajectories exhibited a drift to the right side, and the averaged drift value was 1.82 m. This phenomenon is a result of the systematic modeling error due to the nonzero velocity of the foot during the stance phase, and it was also reported in [24]. Since this drift is the result of a systematic modeling error, it is not within the scope of this article. However, it has been reported that the drift can be eliminated by implementation of two ZUPT-aided navigation systems on two feet and subsequent fusion of the information [38].

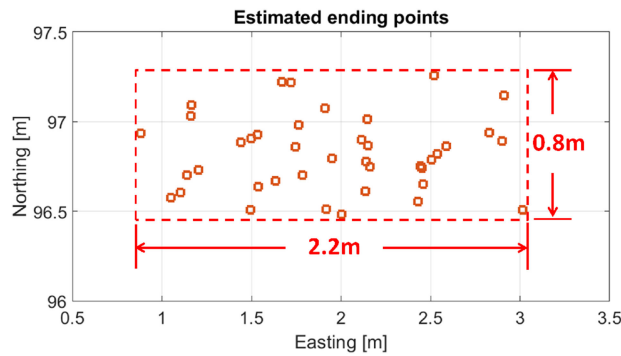


Fig. 9. Ending points of 40 trajectories. All data points lie in a rectangular area with the length of 2.2 m and the width of 0.8 m.

A zoomed-in view of the ending points of 40 trajectories is shown in Fig. 9. The ending points were distributed in a rectangular area with the length of 2.2 m and the width of 0.8 m. Based on IMU performances from Fig. 7 and analytical results from (56) and (57), the uncertainty of position estimation could be calculated as $\sigma_{||} = 0.07$ m and $\sigma_{\perp} = 0.43$ m. Assuming that the position error is normally distributed, 99% of the points should be in an ellipse with the major axis of $6\sigma_{\perp} = 2.58$ m and the minor axis of $6\sigma_{||} = 0.42$ m. The analytical expression was within 20% of the experimental result along the direction perpendicular to the trajectory, showing a good agreement. As for the direction along the trajectory, the analytical result was about 50% smaller than the experimental result, possibly due to the systematic modeling errors. The shock and vibrations of the IMU when the foot touched the ground were also not considered in the analytical model, and it would also introduce extra errors. Similar phenomenon of larger navigation errors with IMU mounted on the foot has been reported previously in [15].

V. CONCLUSION

Estimation errors during ZUPT-aided pedestrian inertial navigation are the result of two main factors: systematic modeling errors and IMU noises. In this article, we presented an analysis on the navigation errors caused by IMU noises. RRW of the gyroscopes was identified as the most dominant error source in the navigation. Analytical expression of the uncertainty of the estimation of angle, velocity, position, and IMU stochastic biases were derived and confirmed with discrepancy of 10% with numerical simulation and 20% with experimental results for the direction perpendicular to the trajectory. We believe that a relatively small discrepancy between the analytical result and the numerical simulation is indicative of the accuracy of the analysis, while a relatively larger discrepancy between the analytical result and the experiments are likely the result of systematic modeling errors, such as biased and correlated process noises, nonlinear navigation dynamics, and the zero-velocity assumption. A possible mitigation solution is to implement adaptive threshold for the ZUPT detector to take advantage of the stance phase, but avoid the

excessive usage of the ZUPT event [39], [40]. This article is envisioned to aid in analysis of the effect of errors in sensors, which might lead to a well-informed selection of sensors for the task of ZUPT-aided pedestrian inertial navigation.

REFERENCES

- [1] X. Yun, E. R. Bachmann, H. Moore, and J. Calusdian, Self-contained position tracking of human movement using small inertial/magnetic sensor modules In *Proc. IEEE Int. Conf. Robot. Autom.*, Roma, Italy, Apr. 10–14, 2007, pp. 2526–2533.
- [2] A. R. Jimenez, F. Seco, C. Prieto, and J. Guevara, A comparison of pedestrian dead-reckoning algorithms using a low-cost MEMS IMU In *Proc. IEEE Int. Symp. Intell. Signal Process.*, Budapest, Hungary, Aug. 26–28, 2009, pp. 37–42.
- [3] K. Shamaei, J. Khalife, and Z. Kassas, Performance characterization of positioning in LTE systems In *Proc. ION GNSS Conf.*, Portland, OR, USA, Sep. 12–16, 2016, pp. 2262–2270.
- [4] K. Nguyen and Z. Luo, Evaluation of bluetooth properties for indoor localisation In *Progress in Location-Based Services*. Berlin, Germany: Springer, 2013, pp. 127–149.
- [5] A. D. J. Ruiz, F. S. Granja, J. C. P. Honorato, and J. I. G. Rosas, Accurate pedestrian indoor navigation by tightly coupling foot-mounted IMU and RFID measurements *IEEE Trans. Instrum. Meas.*, vol. 61, no. 1, pp. 178–189, Jan. 2012.
- [6] D. Titterton and J. Weston, *Strapdown Inertial Navigation Technology*, vol. 207, 2nd ed. Washington, DC, USA: Amer. Inst. Aeronaut. Astronaut., 2004, p. 30.
- [7] M. Ma, Q. Song, Y. Li, and Z. Zhou, A zero velocity intervals detection algorithm based on sensor fusion for indoor pedestrian navigation In *Proc. IEEE Inf. Technol., Netw., Electron. Autom. Control Conf.*, Chengdu, China, Dec. 15–17, 2017, pp. 418–423.
- [8] Y. Geng, R. Martins, and J. Sousa, Accuracy analysis of DVL/IMU/magnetometer integrated navigation system using different IMUs in AUV In *Proc. IEEE Int. Conf. Control Autom.*, Xiamen, China, Jun. 9–11, 2010, pp. 516–521.
- [9] F. Goldenberg, Geomagnetic navigation beyond the magnetic compass In *Proc. IEEE/ION Position, Location, Navigat. Symp.*, Coronado, CA, USA, Apr. 25–27, 2006, pp. 684–694.
- [10] M. Kourogi and T. Kurata, Personal positioning based on walking locomotion analysis with self-contained sensors and a wearable camera In *Proc. IEEE/ACM Int. Symp. Mixed Augmented Reality*, Tokyo, Japan, Oct. 7–10, 2003, pp. 103–112.
- [11] S. Thrun, Simultaneous localization and mapping In *Robotics and Cognitive Approaches to Spatial Mapping*. Berlin, Germany: Springer, 2007, pp. 13–41.
- [12] M. Romanovas *et al.*, Pedestrian indoor localization using foot mounted inertial sensors in combination with a magnetometer, a barometer and RFID In *Progress in Location-Based Services*. Berlin, Germany: Springer, 2013, pp. 151–172.
- [13] J. Parviainen, J. Kantola, and J. Collin, Differential barometry in personal navigation In *Proc. IEEE/ION Position, Location, Navigat. Symp.*, Monterey, CA, USA, May 6–8, 2008, pp. 148–152.

- [14] F. Olsson, J. Rantakokko, and J. Nygard
Cooperative localization using a foot-mounted inertial navigation system and ultrawideband ranging
In *Proc. IEEE Int. Conf. Indoor Positioning Indoor Navigat.*, Busan, South Korea, Oct. 27–30, 2014, pp. 122–131.
- [15] M. Laverne, M. George, D. Lord, A. Kelly, and T. Mukherjee
Experimental validation of foot to foot range measurements in pedestrian tracking
In *Proc. ION GNSS Conf.*, Portland, OR, USA, Sep. 19–23, 2011, pp. 1386–1393.
- [16] Y. Wang, S. Askari, C.-S. Jao, and A. M. Shkel
Directional ranging for enhanced performance of aided pedestrian inertial navigation
In *Proc. IEEE Int. Symp. Inertial Sens. Syst.*, Naples, FL, USA, Apr. 1–5, 2019, pp. 1–2.
- [17] G. Antonelli, F. Arrichiello, S. Chiaverini, and G.-S. Sukhatme
Observability analysis of relative localization for AUVs based on ranging and depth measurements
In *Proc. IEEE Int. Conf. Robot. Autom.*, Anchorage, AK, USA, May 3–7, 2010, pp. 4276–4281.
- [18] E. Foxlin
Pedestrian tracking with shoe-mounted inertial sensors
IEEE Comput. Graph. Appl., vol. 25, no. 6, pp. 38–46, Nov./Dec. 2005.
- [19] L. Ojeda and J. Borenstein
Personal dead-reckoning system for GPS-denied environments
In *Proc. IEEE Int. Workshop Saf., Secur. Rescue Robot.*, Rome, Italy, Sep. 27–29, 2007, pp. 1–6.
- [20] J. O. Nilsson, A. K. Gupta, and P. Handel
Foot-mounted inertial navigation made easy
In *Proc. IEEE Int. Conf. Indoor Positioning Indoor Navigat.*, Busan, South Korea, Oct. 27–30, 2014, pp. 24–29.
- [21] S. Godha and G. Lachapelle
Foot mounted inertial system for pedestrian navigation
Meas. Sci. Technol., vol. 19, no. 7, 2008, Art. no. 075202.
- [22] C. Tjhai and K. O’Keefe
Step-size estimation using fusion of multiple wearable inertial sensors
In *Proc. IEEE Int. Conf. Indoor Positioning Indoor Navigat.*, Sapporo, Japan, Sep. 18–21, 2017, pp. 18–21.
- [23] A. Ramanandan, A. Chen, and J. A. Farrell
Inertial navigation aiding by stationary updates
IEEE Trans. Intell. Transp. Syst., vol. 13, no. 1, pp. 235–248, Mar. 2012.
- [24] J. O. Nilsson, I. Skog, and P. Handel
A note on the limitations of ZUPTs and the implications on sensor error modeling
In *Proc. IEEE Int. Conf. Indoor Positioning Indoor Navigat.*, Sydney, Australia, Nov. 13–15, 2012, pp. 1–4.
- [25] J. O. Nilsson, I. Skog, and P. Handel
Performance characterisation of foot-mounted ZUPT-aided INSs and other related systems
In *Proc. IEEE Int. Conf. Indoor Positioning Indoor Navigat.*, Zurich, Switzerland, Sep. 15–17, 2010, pp. 1–7.
- [26] P. G. Savage
Strapdown Analytics, 2nd ed. Maple Plain, MN, USA: Strapdown Associates, 2007.
- [27] J. K. Huddle
Theory and performance for position and gravity survey with an inertial system
J. Guid., Control, Dyn., vol. 1, no. 3, pp. 183–188, 1978.
- [28] I. Skog, P. Handel, J. O. Nilsson, and J. Rantakokko
Zero-velocity detection—An algorithm evaluation
IEEE Trans. Biomed. Eng., vol. 57, no. 11, pp. 2657–2666, Nov. 2010.
- [29] Y. Wang, S. Askari, and A. M. Shkel
Study on mounting position of IMU for better accuracy of ZUPT-aided pedestrian inertial navigation
In *Proc. IEEE Int. Symp. Inertial Sens. Syst.*, Naples, FL, USA, Apr. 1–5, 2019, pp. 1–4.
- [30] M. Ren, K. Pan, Y. Liu, H. Guo, X. Zhang, and P. Wang
A novel pedestrian navigation algorithm for a foot-mounted inertial-sensor-based system
Sensors, vol. 16, no. 1, 2016, Art. no. 139.
- [31] I. Skog, J. O. Nilsson, and P. Handel
Evaluation of zero-velocity detectors for foot-mounted inertial navigation systems
In *Proc. IEEE Int. Conf. Indoor Positioning Indoor Navigat.*, Zurich, Switzerland, Sep. 15–17, 2010, pp. 1–6.
- [32] A. R. Jimenez, F. Seco, J. C. Prieto, and J. Guevara
Indoor pedestrian navigation using an INS/EKF framework for yaw drift reduction and a foot-mounted IMU
In *Proc. IEEE Workshop Positioning Navigation Commun.*, Dresden, Germany, Mar. 11–12, 2010, pp. 135–143.
- [33] Y. Wang, D. Vatanparvar, A. Chernyshoff, and A. M. Shkel
Analytical closed-form estimation of position error on ZUPT-aided pedestrian inertial navigation
IEEE Sens. Lett., vol. 2, no. 4, Dec. 2018, Art. no. 7001604.
- [34] M. P. Murray, A. B. Drought, and R. C. Kory
Walking gait of normal man
J. Bone Joint Surgery, vol. 46, pp. 335–360, 1964.
- [35] Y. Wang, A. Chernyshoff, and A. M. Shkel
Error analysis of ZUPT-aided pedestrian inertial navigation
In *Proc. IEEE Int. Conf. Indoor Positioning Indoor Navigat.*, Nantes, France, Sep. 24–27, 2018, pp. 206–212.
- [36] N. El-Sheimy, H. Hou, and X. Niu
Analysis and modeling of inertial sensors using Allan variance
IEEE Trans. Instrum. Meas., vol. 57, no. 1, pp. 140–149, Jan. 2008.
- [37] VectorNav VN-200 GPS-Aided Inertial Navigation System Product Brief. [Online]. Available: https://www.vectornav.com/docs/default-source/documentation/vn-200-documentation/PB-12-0003.pdf?sfvrsn=749ee6b9_13. Accessed on: May 12, 2019.
- [38] I. Skog, J. O. Nilsson, D. Zachariah, and P. Handel
Fusing the information from two navigation systems using an upper bound on their maximum spatial separation
In *Proc. IEEE Int. Conf. Indoor Positioning Indoor Navigat.*, Sydney, Australia, Nov. 13–15, 2012, pp. 1–5.
- [39] J. Wahlstrom, I. Skog, F. Gustafsson, A. Markham, and N. Trigoni
Zero-velocity detection—A Bayesian approach to adaptive thresholding
IEEE Sens. Lett., vol. 3, no. 6, Jun. 2019, Art. no. 7000704.
- [40] Y. Wang and A. M. Shkel
Adaptive threshold for zero-velocity detector in ZUPT-aided pedestrian inertial navigation
IEEE Sens. Lett., vol. 3, no. 11, Nov. 2019, Art. no. 7002304.



Yusheng Wang (S'18) received the B.Eng. (Hons.) degree in engineering mechanics from Tsinghua University, Beijing, China, in 2014, and the M.S. degree in mechanical engineering in 2016 from the University of California, Irvine, CA, USA, where he is currently working toward the Ph.D. degree with Microsystems Laboratory.

His research interests include MEMS inertial sensors, strapdown inertial navigation, aiding techniques for navigation, and sensor fusion.

Mr. Wang is a recipient of the 2016–2017 Paul and Beverly Holmes Fellowship and the Best Student Paper Award at the 2019 IEEE International Symposium on Inertial Sensors and Systems. He serves as a Reviewer for the *IEEE Journal of Microelectromechanical Systems* (JMEMS), IEEE JMEMS LETTERS, IEEE SENSORS LETTER, and IEEE COMMUNICATIONS LETTERS.



Andrei Chernyshoff received the Ph.D. degree in mechanical and aerospace engineering from the University of California, Irvine, CA, USA, in 1997.

He is currently consulting with L3 Technologies, Anaheim, CA. His research interests include design of navigation systems for various applications, design of inertial sensors, and signal processing.



Andrei M. Shkel (F'99) received the Diploma (Hons.) degree in mechanics and mathematics from Lomonosov Moscow State University, Moscow, Russia, in 1991, and the Ph.D. degree in mechanical engineering from the University of Wisconsin, Madison, WI, USA, in 1997.

In 2000, he joined the Faculty of the University of California at Irvine (UCI), Irvine, CA, USA, where he is currently a Professor with the Department of Mechanical and Aerospace Engineering, with joint appointments with the Department of Electrical Engineering and Computer Science and the Department of Biomedical Engineering. He served as a Program Manager of Microsystems Technology Office, Defense Advanced Research Projects Agency, Arlington, VA, USA, from 2009 to 2013. He holds more than 40 U.S. and worldwide patents. His research interests, reflected in more than 250 publications, include solid-state sensors and actuators, microelectromechanical-system-based neuroprosthetics, sensor-based intelligence, and control theory.

Dr. Shkel was a recipient of the 2002 George E. Brown, Jr., Award, the 2005 National Science Foundation CAREER Award, the 2006 UCI HSSoE Best Faculty Research Award, and the 2009 IEEE Sensors Council Technical Achievement Award. He received the Office of the Secretary of the Defense Medal for Exceptional Public Service. He served as the Founding Chair of the IEEE International Symposium on Inertial Sensors and Systems. From 2020 to 2022, he will be the President of the IEEE Sensors Council. He has served on a number of Editorial Boards, most recently, as an Editor for the IEEE/ASME JOURNAL OF MICROELECTROMECHANICAL SYSTEMS.